Monthly Notices
of the
ROYAL ASTRONOMICAL SOCIETY

Mon. Not. R. Astron. Soc. **422,** 2465–2473 (2012) doi:10.1111/j.1365-2966.2012.20801.x

Negative effective magnetic pressure in turbulent convection

P. J. Käpylä,[1,2★] A. Brandenburg,[2,3] N. Kleeorin,[2,4] M. J. Mantere[1] and I. Rogachevskii[2,4]

[1]*Department of Physics, University of Helsinki, Gustaf Hällströmin katu 2a (PO Box 64), FI-00064 Helsinki, Finland*
[2]*NORDITA, AlbaNova University Center, Roslagstullsbacken 23, SE-10691 Stockholm, Sweden*
[3]*Department of Astronomy, AlbaNova University Center, Stockholm University, SE-10691 Stockholm, Sweden*
[4]*Department of Mechanical Engineering, Ben-Gurion University of the Negev, PO Box 653, Beer-Sheva 84105, Israel*

Accepted 2012 February 22. Received 2012 February 21; in original form 2011 April 23

ABSTRACT

We investigate the effects of weakly and strongly stratified turbulent convection on the mean effective Lorentz force, and especially on the mean effective magnetic pressure. Earlier studies with isotropically forced non-stratified and stratified turbulence have shown that the contribution of the turbulence to the mean magnetic pressure is negative for mean horizontal magnetic fields that are smaller than the equipartition strength, so that the effective mean magnetic pressure that takes into account the turbulence effects can be negative. Compared with earlier cases of forced turbulence with an isothermal equation of state, we find that the turbulence effect is similar to or even stronger in the present case of turbulent convection. This is argued to be due to the anisotropy of turbulence in the vertical direction. Another important difference compared with earlier studies is the presence of an evolution equation for the specific entropy. Mean-field modelling with entropy evolution indicates that the negative effective magnetic pressure can still lead to a large-scale instability which forms local flux concentrations, even though the specific entropy evolution tends to have a stabilizing effect when applied to a stably stratified (e.g. isothermal) layer. It is argued that this large-scale instability could be important for the formation of solar large-scale magnetic structures such as active regions.

Key words: convection – hydrodynamics – magnetic fields – MHD – turbulence.

1 INTRODUCTION

The spatial and temporal coherence of the large-scale magnetic field of the Sun is manifested by sunspots appearing within a certain range of latitudes from one cycle to the next. A hydromagnetic dynamo is commonly held responsible for the generation and maintenance of large-scale magnetic fields (cf. Moffatt 1978; Parker 1979; Krause & Rädler 1980; Rüdiger & Hollerbach 2004; Brandenburg & Subramanian 2005). Some models (Parker 1955, 1982, 1984; Spiegel & Weiss 1980; Spruit 1981; Schüssler et al. 1994; Dikpati & Charbonneau 1999), known as flux transport dynamos, rely on the existence of strong magnetic flux tubes at the base of the convection zone or somewhat below; see also reviews by Hughes (2007) and Tobias & Weiss (2007). These concentrations of the magnetic field are thought to become unstable once the field strength exceeds a critical value. The subsequent rise of magnetic flux tubes to the surface is used to explain active regions and sunspots. Such models, however, face a number of serious issues: first, the required strength of the magnetic flux tubes is of the order of 10^5 G (D'Silva & Choudhuri 1993), which is expected to be a hundred times the equipartition strength which is at odds with estimates that the tachocline becomes unstable already when fields of the order of 10^3 G are present (e.g. Arlt, Sule & Rüdiger 2005). Such strong fields are also hard to produce by a turbulent dynamo (Guerrero & Käpylä 2011).

An alternative scenario for the large-scale solar magnetic field is that it is maintained within the convection zone by a distributed dynamo, which generates diffuse sub-equipartition strength magnetic fields (e.g. Stix 1976; Brandenburg 2005; Käpylä, Korpi & Tuominen 2006). Unlike the flux-transport dynamo, a distributed dynamo does not directly explain the existence of sunspots and active regions. The alternative idea that sunspots have their origin within the convection zone and that they might thus be shallow phenomena is supported by observations showing that the rotation rate of the Sun, as measured by sunspots, depends monotonically on their age so that young spots are the fastest and oldest spots are the slowest (Pulkkinen & Tuominen 1998; Brandenburg 2005). If one imagines sunspots floating in the plasma, the rotation rate of the youngest spots corresponds to roughly that at $r = 0.95\,\mathrm{R}_\odot$. The decreasing rotation rate as a function of age is consistent with older spots being anchored at increasingly higher layers where Ω is smaller due to its negative radial gradient near the surface; see fig. 4 of

★E-mail: petri.kapyla@helsinki.fi

Benevolenskaya et al. (1999). This suggests that sunspots may form near the surface of the Sun rather than through the buoyant rise of coherent flux tubes from the tachocline. This is therefore compatible with the distributed dynamo picture provided the diffuse fields within the convection zone can form concentrations like sunspots near the surface (Brandenburg 2005).

A promising mechanism that can form strong concentrations from an initially uniform magnetic field was suggested by Kleeorin et al. (1989) and Kleeorin, Rogachevskii & Ruzmaikin (1990) who considered the effects of turbulence or turbulent convection on the large-scale Lorentz force. This work has been elaborated upon in a number of subsequent papers (Kleeorin & Rogachevskii 1994; Kleeorin, Mond & Rogachevskii 1996; Rogachevskii & Kleeorin 2007). They find that, for a given range of large-scale magnetic field strengths, there is a negative turbulence contribution to the mean magnetic pressure, and the effective mean magnetic pressure that accounts for the turbulence effects can be negative. This results in an excitation of a large-scale instability. The growth rate of the instability increases as a function of density stratification (Kemel et al. 2012b). In the Sun the density drops steeply in the outermost layers, which favours the development of this instability there.

The strongly stratified large-eddy simulations of Ustyugov (2009) and Kitiashvili et al. (2010) may already have detected magnetic flux concentrations in turbulent convection formed from initially uniform vertical magnetic fields. Note also that a segregation into strongly and weakly magnetized regions in magneto-convection has been observed in numerical simulations at large aspect ratios by Tao et al. (1998) and Tian & Petrovay (2012), which may have its origin in some mean-field effect of the type considered here. Also, simulations of Stein et al. (2011) with a horizontal uniform field at the bottom of the domain show emergence of magnetic flux structures, while a number of numerical studies (e.g. Schüssler & Vögler 2006; Martínez, Hansteen & Carlson 2008; Rempel, Schüssler & Knölker 2009) use strongly non-uniform fields as initial or boundary conditions. The origin of such non-uniform fields is therefore not addressed in these latter studies.

Direct numerical simulations (DNS) of homogeneous (Brandenburg, Kleeorin & Rogachevskii 2010, hereafter BKR) and density stratified (Brandenburg et al. 2012, hereafter BKKR) forced turbulence have shown that the effective magnetic pressure is negative for field strengths below about 40 per cent of the equipartition value, provided the magnetic Reynolds number exceeds unity. However, definitive proof of an instability associated with the negative effective magnetic pressure phenomenon came only more recently with DNS of forced turbulence that have sufficiently many turbulent eddies in the simulation domain (Brandenburg et al. 2011; Kemel et al. 2012a). This work has only become possible due to earlier DNS (BKR; Kemel et al. 2012b) exploring first the relevant parameter regime. In the present study, we investigate the effect of turbulent convection on the effective mean Lorentz force in DNS and study the formation of large-scale magnetic structures in mean-field models.

2 EFFECTIVE MEAN LORENTZ FORCE

In this section we state the underlying equations, highlighting the difference to earlier work where anisotropic contributions from gravity were either weak or absent.

2.1 Governing equations

In this study we are mainly interested in the effects of turbulent convection on the mean Lorentz force. To this end, we consider the momentum equation

$$\frac{\partial}{\partial t}\rho\, U_i = -\frac{\partial}{\partial x_j}\Pi_{ij} + \rho g_i, \tag{1}$$

where $\boldsymbol{g}$ is the acceleration due to gravity,

$$\Pi_{ij} = \rho\, U_i U_j + \delta_{ij}\left(p + \frac{1}{2}\boldsymbol{B}^2\right) - B_i B_j - 2\nu\rho\, \boldsymbol{S}_{ij} \tag{2}$$

is the momentum stress tensor, $\boldsymbol{U}$ and $\boldsymbol{B}$ are the velocity and magnetic fields, p and ρ are the fluid pressure and density, δ_{ij} is the Kronecker tensor, ν is the kinematic viscosity, and

$$\boldsymbol{S}_{ij} = \frac{1}{2}(\partial_i U_j + \partial_j U_i) - \frac{1}{3}\delta_{ij}\nabla\cdot\boldsymbol{U} \tag{3}$$

is the trace-free rate of strain tensor. Throughout this paper, we have adopted units where the vacuum permeability μ_0 is set to unity, although we do include it in some expressions for clarity.

Neglecting correlations between velocity and density fluctuations for low-Mach number turbulence, the averaged momentum equation is

$$\frac{\partial}{\partial t}\overline{\rho}\,\overline{U}_i = -\frac{\partial}{\partial x_j}\overline{\Pi}_{ij} + \overline{\rho}\, g_i, \tag{4}$$

where $\overline{\rho}$ is the mean fluid density, $\overline{\boldsymbol{U}}$ is the mean fluid velocity, $\overline{\Pi}_{ij} = \overline{\Pi}^{\rm m}_{ij} + \overline{\Pi}^{\rm f}_{ij}$ is the mean momentum stress tensor split into contributions resulting entirely from the mean field (indicated by superscript m) and those of the fluctuating field (indicated by superscript f). The tensor $\overline{\Pi}^{\rm m}_{ij}$ has the same form as equation (2), but all quantities have now attained an overbar, i.e.

$$\overline{\Pi}^{\rm m}_{ij} = \overline{\rho}\,\overline{U}_i\overline{U}_j + \delta_{ij}\left(\overline{p} + \frac{1}{2}\overline{\boldsymbol{B}}^2\right) - \overline{B}_i\overline{B}_j - 2\nu\overline{\rho}\,\overline{\boldsymbol{S}}_{ij}, \tag{5}$$

where $\overline{\boldsymbol{B}}$ is the mean magnetic field and $\overline{p}$ is the mean fluid pressure. The contributions, $\overline{\Pi}^{\rm f}_{ij}$, which result from the fluctuations of velocity $\boldsymbol{u} = \boldsymbol{U} - \overline{\boldsymbol{U}}$ and magnetic fields $\boldsymbol{b} = \boldsymbol{B} - \overline{\boldsymbol{B}}$, are determined by

$$\overline{\Pi}^{\rm f}_{ij} = \overline{\rho}\,\overline{u_i u_j} + \frac{1}{2}\delta_{ij}\overline{\boldsymbol{b}^2} - \overline{b_i b_j}. \tag{6}$$

This contribution, together with the one from the mean field, $\overline{\Pi}^{\rm m}_{ij}$, comprises the total mean momentum tensor. The contribution from the fluctuating fields is split into parts that are independent of the mean magnetic field (which determine the turbulent viscosity and background turbulent pressure) and parts that do depend on the mean magnetic field.

In the present study, we consider turbulent convection with an imposed uniform horizontal magnetic field, $\boldsymbol{B}_0 = (B_0, 0, 0)$, that is perpendicular to the direction of gravity. This modifies the stress tensor from $\overline{\Pi}^{\rm f,0}_{ij}$ to $\overline{\Pi}^{\rm f,\overline{B}}_{ij}$, so only the difference,

$$\Delta\overline{\Pi}^{\rm f}_{ij} \equiv \overline{\Pi}^{\rm f,\overline{B}}_{ij} - \overline{\Pi}^{\rm f,0}_{ij}, \tag{7}$$

depends on the mean magnetic field $\overline{\boldsymbol{B}}$ and can be parametrized as (Rogachevskii & Kleeorin 2007)

$$\Delta\overline{\Pi}^{\rm f}_{ij} = q_{\rm s}\overline{\boldsymbol{B}}^2\hat{B}_i\hat{B}_j - \left(\frac{1}{2}q_{\rm p}\,\delta_{ij} + q_{\rm g}\,\hat{g}_i\hat{g}_j\right)\overline{\boldsymbol{B}}^2, \tag{8}$$

where $\hat{\boldsymbol{g}}$ is the vertical unit vector directed along the gravity field, $\hat{B}_j = \overline{B}_j/\overline{B}$ is the unit vector directed along the mean magnetic field, $q_{\rm s}$, $q_{\rm p}$ and $q_{\rm g}$ are functions of magnetic Reynolds and Prandtl numbers as well as the modulus of the normalized mean field,

$$\beta = \overline{B}/B_{\rm eq}, \quad \text{where} \quad \overline{B} = |\overline{\boldsymbol{B}}|, \quad \text{and} \quad B_{\rm eq} = (\overline{\rho\boldsymbol{u}^2})^{1/2} \tag{9}$$

is the equipartition field strength. To derive equation (8), we use equations (A22)–(A24) of Rogachevskii & Kleeorin (2007). The

parametrization (8) also follows from symmetry arguments which allow us to construct a symmetric tensor with two preferential perpendicular directions along the horizontal magnetic field $\hat{\boldsymbol{B}}$ and vertical gravity field $\hat{\boldsymbol{g}}$. Such symmetric tensor is a linear combination of symmetric tensors δ_{ij}, $\hat{B}_i\hat{B}_j$ and $\hat{g}_i\hat{g}_j$. (In the case of an oblique imposed magnetic field, there would be an additional contribution.)

The effective mean Lorentz force that takes into account the turbulent convection effects reads

$$\begin{aligned}\overline{\rho}\,\overline{\mathcal{F}}_i^{\rm M} &= -\nabla_j\left(\frac{1}{2}\overline{\boldsymbol{B}}^2\delta_{ij}-\overline{B}_i\overline{B}_j+\Delta\overline{\Pi}_{ij}^{\rm f}\right)\\ &= -\frac{1}{2}\nabla_i\left[(1-q_{\rm p})\,\overline{\boldsymbol{B}}^2\right]+\hat{g}_i\,\nabla_z\left(q_{\rm g}\,\overline{\boldsymbol{B}}^2\right)\\ &\quad+\overline{\boldsymbol{B}}\cdot\nabla\left[(1-q_{\rm s})\,\overline{\boldsymbol{B}}\right].\end{aligned}\tag{10}$$

The analytic expressions for the non-linear quenching functions, $q_{\rm p}(\beta)$, $q_{\rm s}(\beta)$ and $q_{\rm g}(\beta)$, for turbulent convection have been derived in Rogachevskii & Kleeorin (2007). Their asymptotic formulae are given below. For weak mean magnetic fields, $4\beta \ll R_{\rm m}^{-1/4}$, the functions $q_{\rm p}$, $q_{\rm s}$ and $q_{\rm g}$ are given by

$$q_{\rm p}(\beta)=\frac{4}{5}\left(\ln R_{\rm m}+\frac{4}{45}\right)-\frac{7}{3}\,a_*+\frac{16\,\ell_0^2}{9\,H_\rho^2},$$

$$q_{\rm s}(\beta)=\frac{8}{15}\left(\ln R_{\rm m}+\frac{2}{15}\right),\quad q_{\rm g}(\beta)=8a_*-\frac{8\,\ell_0^2}{3\,H_\rho^2};$$

for $R_{\rm m}^{-1/4}\ll 4\beta\ll 1$, these functions are

$$q_{\rm p}(\beta)=\frac{16}{25}\left[5|\ln(4\beta)|+1+32\,\beta^2\right]-\frac{7}{3}\,a_*+\frac{16\,\ell_0^2}{9\,H_\rho^2},$$

$$q_{\rm s}(\beta)=\frac{32}{15}\left[|\ln(4\beta)|+\frac{1}{30}+12\beta^2\right],$$

$$q_{\rm g}(\beta)=8a_*-\frac{8\,\ell_0^2}{3\,H_\rho^2},$$

while for strong fields, $4\beta\gg 1$, they are

$$q_{\rm p}(\beta)=\frac{1}{6\beta^2}\left(1+\frac{3\,\ell_0^2}{H_\rho^2}\right)+\frac{\pi a_*}{80\beta},$$

$$q_{\rm s}(\beta)=\frac{\pi}{48\beta^3}+\frac{3\pi a_*}{160\beta},\quad q_{\rm g}(\beta)=\frac{3\pi a_*}{40\beta^3}-\frac{3\,\ell_0^2}{4\,H_\rho^2\,\beta^2}.$$

Here, $R_{\rm m}=\ell_0\,u_{\rm ums}/\eta$ is the magnetic Reynolds number based on the integral scale of turbulent convection, ℓ_0, and the root-mean-square (rms) value of the velocity, $u_{\rm rms}$, η is the magnetic diffusion due to the electrical conductivity of the fluid, and H_ρ is the density scale height. The parameter a_* characterizes turbulent convection and is determined from the budget equation for the total energy, yielding

$$a_*^{-1}=1+\left[\nu_{\rm t}(\nabla\overline{\boldsymbol{U}})^2+\eta_{\rm t}(\nabla\overline{\boldsymbol{B}})^2/\rho\right]/gF_*,$$

where $\nu_{\rm t}$ is the turbulent viscosity, $\eta_{\rm t}$ is the turbulent magnetic diffusivity, $F_*=\overline{u_z\,s'}$ is the vertical heat flux from the background turbulent convection, and s' are fluctuations of the specific entropy.

2.2 Turbulent contributions to effective Lorentz force

To study the effects of turbulent convection on the Reynolds and Maxwell stresses, and hence on the effective Lorentz force from the mean field, we need to determine the functions $q_{\rm p}(\beta)$, $q_{\rm s}(\beta)$ and $q_{\rm g}(\beta)$ in DNS. Allowing here for the possibility of small-scale dynamo action, equations (6)–(8) yield

$$\begin{aligned}&\Delta\overline{\rho u_i u_j}+\frac{1}{2}\delta_{ij}\Delta\overline{\boldsymbol{b}^2}-\Delta\overline{b_i b_j}\\ &\quad=\left[q_{\rm s}\hat{B}_i\hat{B}_j-\left(\frac{1}{2}q_{\rm p}\,\delta_{ij}+q_{\rm g}\,\hat{g}_i\,\hat{g}_j\right)\right]\overline{\boldsymbol{B}}^2.\end{aligned}\tag{11}$$

Here, $\Delta\overline{\rho u_i u_j}=\overline{\rho u_i u_j}-\overline{\rho u_{0i}u_{0j}}$ and $\Delta\overline{b_i b_j}=\overline{b_i b_j}-\overline{b_{0i}b_{0j}}$, where subscripts 0 indicate values in the absence of the mean magnetic field. To obtain thee independent equations for the three unknowns, we multiply equation (11):

(i) by $\hat{g}_i\,\hat{g}_j$,

$$\Delta\overline{\rho u_z^2}+\frac{1}{2}\Delta\overline{\boldsymbol{b}^2}-\Delta\overline{b_z^2}=-\left(\frac{1}{2}q_{\rm p}+q_{\rm g}\right)\overline{\boldsymbol{B}}^2,\tag{12}$$

(ii) by $\hat{B}_i\hat{B}_j$ (defining $u_{\hat{B}}=\boldsymbol{u}\cdot\hat{\boldsymbol{B}}_0$ and $b_{\hat{B}}=\boldsymbol{b}\cdot\hat{\boldsymbol{B}}_0$):

$$\Delta\overline{\rho u_{\hat{B}}^2}+\frac{1}{2}\Delta\overline{\boldsymbol{b}^2}-\Delta\overline{b_{\hat{B}}^2}=-\left(\frac{1}{2}q_{\rm p}-q_{\rm s}\right)\overline{\boldsymbol{B}}^2,\tag{13}$$

(iii) and compute the trace of equation (11),

$$\Delta\overline{\rho\boldsymbol{u}^2}+\frac{1}{2}\Delta\overline{\boldsymbol{b}^2}=-\left(\frac{3}{2}q_{\rm p}+q_{\rm g}-q_{\rm s}\right)\overline{\boldsymbol{B}}^2.\tag{14}$$

Equations (12)–(14) yield the functions $q_{\rm p}(\beta)$, $q_{\rm s}(\beta)$ and $q_{\rm g}(\beta)$:

$$q_{\rm p}(\beta)\,\overline{B}^2=-2\Delta\overline{\rho u_y^2}-\Delta\overline{\boldsymbol{b}^2}+2\Delta\overline{b_y^2},\tag{15}$$

$$q_{\rm s}(\beta)\,\overline{B}^2=-\Delta\overline{\rho u_y^2}+\Delta\overline{\rho u_x^2}+\Delta\overline{b_y^2}-\Delta\overline{b_x^2},\tag{16}$$

$$q_{\rm g}(\beta)\,\overline{B}^2=-\Delta\overline{\rho u_z^2}+\Delta\overline{\rho u_y^2}+\Delta\overline{b_z^2}-\Delta\overline{b_y^2}.\tag{17}$$

Using equations (15)–(17), we determine the functions $q_{\rm p}(\beta)$, $q_{\rm s}(\beta)$ and $q_{\rm g}(\beta)$ from DNS in Section 3. In all those cases, overbars denote averages over x, y and t during the statistically steady state, corresponding to a time interval Δt of up to a thousand turnover times, i.e. $\Delta t u_{\rm rms}k_f=O(1000)$.

3 DIRECT NUMERICAL SIMULATIONS

3.1 DNS model

We use two different set-ups when studying the effects of convection on the mean Lorentz force: (i) a weakly stratified model, similar to that used in Käpylä, Korpi & Brandenburg (2010), without overshoot layers; and (ii) a strongly stratified set-up, similar to that in Käpylä, Korpi & Brandenburg (2009), including upper and lower overshoot layers. In both cases, we use a Cartesian domain with $L_x=L_y=5d$, where d is the depth of the convectively unstable layer. The convective layer is situated at $0<z<d$ in both set-ups. In the strongly stratified set-up, the z-coordinate runs from $-0.85d<z<1.15$. We solve a set of hydromagnetic equations

$$\frac{\partial\boldsymbol{A}}{\partial t}=\boldsymbol{U}\times\boldsymbol{B}-\eta\mu_0\boldsymbol{J},\tag{18}$$

$$\frac{{\rm D}\boldsymbol{U}}{{\rm D}t}=-\frac{1}{\rho}\nabla p+\boldsymbol{g}+\frac{1}{\rho}\boldsymbol{J}\times\boldsymbol{B}+\frac{1}{\rho}\nabla\cdot2\nu\rho\boldsymbol{S},\tag{19}$$

$$\frac{{\rm D}\ln\rho}{{\rm D}t}=-\nabla\cdot\boldsymbol{U},\tag{20}$$

$$T\frac{{\rm D}s}{{\rm D}t}=\frac{1}{\rho}\nabla\cdot K\nabla T+2\nu\boldsymbol{S}^2+\frac{\eta\mu_0}{\rho}\boldsymbol{J}^2-\Gamma_{\rm cool},\tag{21}$$

where $\mathrm{D}/\mathrm{D}t = \partial/\partial t + \boldsymbol{U}\cdot\nabla$ is the advective time derivative, $\boldsymbol{A}$ is the magnetic vector potential, $\boldsymbol{B} = \nabla\times\boldsymbol{A} + \boldsymbol{B}_0$ is the magnetic field, $\boldsymbol{B}_0 = (B_0, 0, 0)$ is the imposed field, $\boldsymbol{J} = \mu_0^{-1}\nabla\times\boldsymbol{B}$ is the current density, η and ν are the magnetic diffusivity and kinematic viscosity, respectively, K is the heat conductivity, ρ is the density, $\boldsymbol{U}$ is the velocity, s is the specific entropy, and $\boldsymbol{g} = -g\hat{\boldsymbol{z}}$ is the gravitational acceleration. The fluid obeys an ideal gas law $p = \rho e(\gamma - 1)$, where p and e are the pressure and internal energy, respectively, and $\gamma = c_\mathrm{P}/c_\mathrm{V} = 5/3$ is the ratio of specific heats at constant pressure and volume, respectively. The specific internal energy per unit mass is related to the temperature via $e = c_\mathrm{V}T$, and the rate of strain tensor $\boldsymbol{S}$ is given by equation (3). The stratification in the hydrostatic initial state can be described by a polytrope with index $m = 1$ in the weakly stratified case, and the stratified three-layer set-up is described by polytropic indices $(m_1, m_2, m_3) = (3, 1, 1)$. In the latter set-up, a cooling term Γ_cool operates in the region $z > 1$, keeping the layer isothermal. The density contrast across the full domain, $\Delta\rho = \rho_\mathrm{bot}/\rho_\mathrm{top}$, is 1.2 (runs A) and 320 (runs B, see Table 1). In the latter case, the density changes by a factor of roughly 13 within the convectively unstable layer. Typical flow patterns from both set-ups are shown in Fig. 1. In all simulations, we use the PENCIL code.[1]

The horizontal boundaries are periodic. In the weakly stratified case, we keep the temperature fixed at the top and bottom boundaries, whereas in the more strongly stratified set-up the upper boundary is isothermal and a constant flux of energy is applied at the lower boundary by fixing the temperature gradient. For the velocity we apply impenetrable, stress-free conditions according to

$$\partial_z U_x = \partial_z U_y = U_z = 0. \tag{22}$$

For the magnetic field, we use vertical field conditions

$$B_x - B_0 = B_y = 0. \tag{23}$$

Dimensionless quantities are obtained by setting

$$d = g = \rho_0 = c_\mathrm{P} = \mu_0 = 1, \tag{24}$$

where ρ_0 is the fluid density at $z_\mathrm{m} = \frac{1}{2}d$. The units of length, time, velocity, density, specific entropy and magnetic field are then

$$[x] = d, \quad [t] = \sqrt{d/g}, \quad [U] = \sqrt{dg},$$
$$[\rho] = \rho_0, \quad [s] = c_\mathrm{P}, \quad [B] = \sqrt{dg\rho_0\mu_0}. \tag{25}$$

The simulations are controlled by the following dimensionless parameters: thermal and magnetic diffusion in comparison to viscosity are measured by the Prandtl numbers

$$\mathrm{Pr} = \frac{\nu}{\chi_0}, \quad \mathrm{Pm} = \frac{\nu}{\eta}, \tag{26}$$

where $\chi_0 = K/(c_\mathrm{P}\rho_0)$ is the reference value of the thermal diffusion coefficient measured in the middle of the layer (z_m) of the non-convecting hydrostatic reference initial state. The efficiency of convection is characterized by the Rayleigh number

$$\mathrm{Ra} = \frac{gd^4}{\nu\chi_0}\left(-\frac{1}{c_\mathrm{P}}\frac{\mathrm{d}s}{\mathrm{d}z}\right)_{z_\mathrm{m}}, \tag{27}$$

which is again determined from the initial non-convecting state at z_m. The entropy gradient can be presented in terms of logarithmic temperature gradients

$$\left(-\frac{1}{c_\mathrm{P}}\frac{\mathrm{d}s}{\mathrm{d}z}\right)_{z_\mathrm{m}} = \frac{\nabla - \nabla_\mathrm{ad}}{H_\mathrm{P}}, \tag{28}$$

[1] http://pencil-code.googlecode.com

Table 1. Summary of the runs. Here, $\mathrm{Ma} = u_\mathrm{rms}/\sqrt{dg}$, and the imposed field in normalized form is given by $\tilde{B}_0 = B_0/B_\mathrm{eq}$, where B_eq is the volume-averaged equipartition field. The last column gives the density contrast, $\Delta\rho$, over the entire domain. The Prandtl number is equal to unity in all runs. We use grid resolutions $128^2\times 64$ (runs A1–A24), $256^2\times 128$ (runs A25–A29) and $256^2\times 192$ (runs B1–B8).

Run	Ma	Ra	Rm	Pm	$\tilde{B}_0$	$\Delta\rho$
A0h	0.068	10^6	–	–	–	1.2
A1	0.068	10^6	11	0.2	0.07	1.2
A2	0.066	10^6	11	0.2	0.15	1.2
A3	0.059	10^6	9	0.2	0.34	1.2
A4	0.055	10^6	9	0.2	0.54	1.2
A5	0.052	10^6	8	0.2	0.78	1.2
A6	0.053	10^6	8	0.2	0.95	1.2
A7	0.059	10^6	9	0.2	1.17	1.2
A8	0.066	10^6	11	0.2	1.52	1.2
A9	0.068	10^6	22	0.4	0.07	1.2
A10	0.065	10^6	21	0.4	0.15	1.2
A11	0.055	10^6	18	0.4	0.36	1.2
A12	0.051	10^6	16	0.4	0.59	1.2
A13	0.048	10^6	15	0.4	0.83	1.2
A14	0.059	10^6	16	0.4	1.01	1.2
A15	0.061	10^6	19	0.4	1.15	1.2
A16	0.066	10^6	21	0.4	1.51	1.2
A17	0.065	10^6	51	1.0	0.08	1.2
A18	0.061	10^6	49	1.0	0.16	1.2
A19	0.051	10^6	41	1.0	0.39	1.2
A20	0.047	10^6	37	1.0	0.64	1.2
A21	0.047	10^6	37	1.0	0.86	1.2
A22	0.050	10^6	39	1.0	1.01	1.2
A23	0.059	10^6	47	1.0	1.18	1.2
A24	0.069	10^6	55	1.0	1.46	1.2
A25h	0.058	4.2×10^6	–	–	–	1.2
A25	0.058	4.2×10^6	92	1.0	0.09	1.2
A26	0.044	4.2×10^6	70	1.0	0.46	1.2
A27	0.040	4.2×10^6	63	1.0	0.76	1.2
A28	0.042	4.2×10^6	66	1.0	0.96	1.2
A29	0.047	4.2×10^6	75	1.0	1.07	1.2
B0h	0.032	1.2×10^7	–	–	–	320
B1	0.032	1.2×10^7	51	1.0	0.01	320
B2	0.031	1.2×10^7	49	1.0	0.07	320
B3	0.028	1.2×10^7	45	1.0	0.23	320
B4	0.027	1.2×10^7	43	1.0	0.32	320
B5	0.027	1.2×10^7	43	1.0	0.41	320
B6	0.026	1.2×10^7	42	1.0	0.61	320
B7	0.025	1.2×10^7	40	1.0	0.78	320
B8	0.025	1.2×10^7	40	1.0	0.92	320

with $\nabla = (\partial\ln T/\partial\ln p)_{z_\mathrm{m}}$, $\nabla_\mathrm{ad} = 1 - 1/\gamma$, and H_P being the pressure scale height at $z = z_\mathrm{m}$.

The effects of viscosity and magnetic diffusion are quantified respectively by the fluid and magnetic Reynolds numbers

$$\mathrm{Re} = \frac{u_\mathrm{rms}}{\nu k_f}, \quad \mathrm{Rm} = \frac{u_\mathrm{rms}}{\eta k_f} = \mathrm{Pm}\,\mathrm{Re}, \tag{29}$$

where u_rms is the rms value of the velocity and $k_f = 2\pi/d$ is the wavenumber corresponding to the depth of the convectively unstable layer. Again, it is convenient to measure the magnetic field strength in terms of the equipartition value. The values of these parameters used in different runs are given in Table 1.

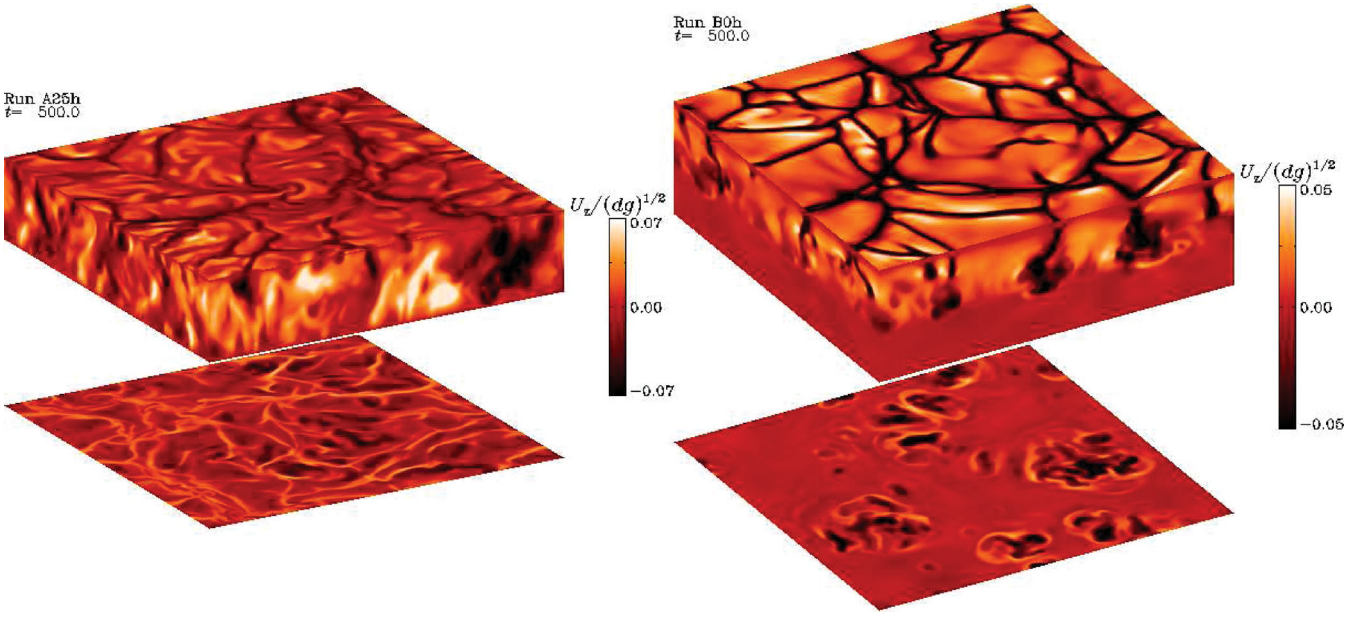

Figure 1. Velocity component U_z at the periphery of the domain from hydrodynamical runs A25h ($\Delta\rho = 1.2$, left) and B0h ($\Delta\rho = 320$, right). In both cases the top and bottom slices show U_z near the top and bottom of the convectively unstable layer, respectively.

3.2 Effective mean Lorentz force from DNS

We now turn to DNS models of turbulent convection to determine the coefficients q_p, q_s and q_g using equations (15)–(17). First, we perform purely hydrodynamical simulations to determine the turbulent background velocity $\overline{\boldsymbol{u}}^2$ in the absence of magnetic fields. No dynamo action occurs in runs A1–A16 and B1–B8, whereas in runs A17–A24 the dynamo is growing very slowly, and in A25–A29 a small-scale dynamo is operating. We find that the critical Rm for Pm = 1 is between 50 and 60, which is almost two times higher than in the case Pm = 5 studied earlier (Käpylä, Korpi & Brandenburg 2008). The hydrodynamical simulations have been run sufficiently long (roughly 250 turnover times) so that it is thermally relaxed and the turbulence is statistically steady. The last snapshot of the hydrodynamical run is used as the initial condition for all subsequent simulations where a uniform magnetic field is imposed.

Next, we consider an imposed horizontal field, $\boldsymbol{B}_0 = (B_0, 0, 0)$. Earlier numerical studies have shown that the effective mean magnetic pressure that takes into account turbulence effects is negative when the mean magnetic fields are smaller than the equipartition strength in non-stratified (BKR) and stratified (BKKR) forced turbulence. In the present study we investigate this issue for turbulent convection with weak and strong density stratification. Let us define the dimensionless effective mean magnetic pressure $\mathcal{P}_{\rm eff}$ as

$$\mathcal{P}_{\rm eff} = \frac{1}{2}(1 - q_p)\overline{\boldsymbol{B}}^2/B_{\rm eq}^2, \tag{30}$$

where $q_p = q_p(\overline{B}/B_{\rm eq})$ and $B_{\rm eq} = B_{\rm eq}(z)$. Following earlier work (BKKR; Kemel et al. 2012a), we characterize our numerical results for q_p by a fit of the form

$$q_p = \frac{q_{p0}}{1 + \boldsymbol{B}^2/B_p^2}, \tag{31}$$

where q_{p0} and B_p are fit parameters, which are determined by matching the shape of $\mathcal{P}_{\rm eff}$ near its minimum and where $\mathrm{d}\mathcal{P}_{\rm eff}/\mathrm{d}\overline{B}^2 < 0$, which is the range relevant to the negative magnetic pressure instability (Rogachevskii & Kleeorin 2007; BKKR). We also use the same ansatz for q_s and q_g, and define in this way the fit parameters

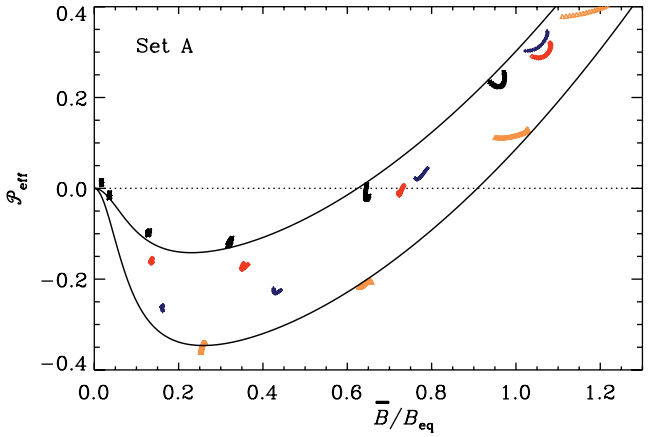

Figure 2. Effective magnetic pressure as a function of the mean magnetic field from weakly stratified runs A1–A29 with an imposed horizontal field $\boldsymbol{B}_0 = B_0\hat{\boldsymbol{x}}$. The black stars, red diamonds, blue crosses and yellow triangles denote simulations with Rm $\approx$ 10, 20, 50 and 70, respectively. We omit points near the boundaries at $z/d < 0.35$ and $z/d > 0.65$. The two curves correspond to approximate fits determined by equation (31), with $q_{p0} = 40$ and $B_p = 0.1B_{\rm eq}$ (upper curve, small Rm), and $q_{p0} = 130$ and $B_p = 0.08B_{\rm eq}$ (lower curve, larger Rm), respectively.

q_{s0}, q_{g0}, B_s and B_g. Note that, due to turbulent pumping effects, the mean magnetic field $\overline{\boldsymbol{B}}$ in general also depends on height – even in the absence of a large-scale dynamo; see Käpylä et al. (2010) and BKKR.

Results for the effective mean magnetic pressure $\mathcal{P}_{\rm eff}$ from weakly and strongly stratified runs are shown in Figs 2–3. Since $\overline{\boldsymbol{B}}$ and $B_{\rm eq}$ are functions of z, we obtain for each combination of imposed field strength and Rm a family of solutions for q_p, q_s and q_g. We neglect points near the top and bottom boundaries to avoid boundary effects. The result is shown in Fig. 2. For weak stratification (runs A1–A29), a negative contribution of turbulent convection to the mean magnetic pressure is found if the mean magnetic field is smaller than the equipartition value. The maximum of this contribution is

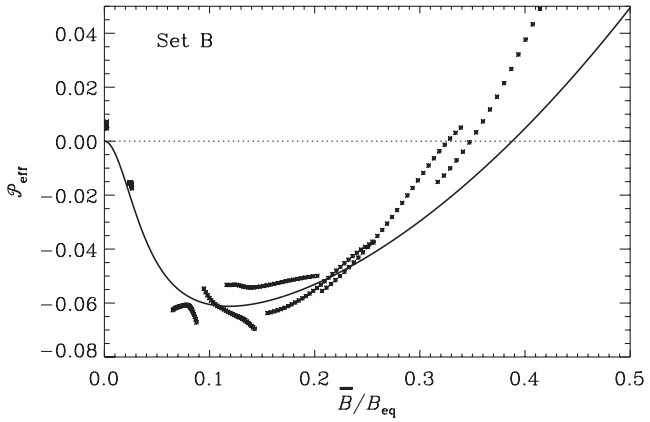

Figure 3. Same as Fig. 2 but for runs B1–B8 for Rm = 40–50. The solid line corresponds to a fit with $q_{\rm p0} = 95$ and $B_{\rm p} = 0.04B_{\rm eq}$.

attained near $\overline{\boldsymbol{B}} \approx 0.5B_{\rm eq}\hat{\boldsymbol{x}}$ and it tends to be somewhat stronger for larger magnetic Reynolds number.

In the strongly stratified runs (see Fig. 3), we also find a negative contribution of turbulent convection to the mean magnetic pressure, but it is constrained to somewhat lower values ($\overline{\boldsymbol{B}} < 0.4B_{\rm eq}\hat{\boldsymbol{x}}$) of the mean magnetic field, and the effective mean magnetic pressure, $\mathcal{P}_{\rm eff}$, has a weaker minimum than in the weakly stratified case. It appears that we find universal scaling for $\mathcal{P}_{\rm eff}$ as a function of $\overline{\boldsymbol{B}}/B_{\rm eq}$ as was obtained in BKKR for stratified forced turbulence, provided that only data points near the middle ($0.35 < z/d < 0.65$) of the convectively unstable layer are used. Furthermore, our highly stratified simulations show that the minimum of $\mathcal{P}_{\rm eff}$ and the range of the mean magnetic field in which $\mathcal{P}_{\rm eff}$ is negative are roughly consistent with those found by BKKR.

Due to anisotropy of turbulent convection, there is a significant contribution to the effective mean magnetic pressure characterized by the term $q_{\rm g}$. This function affects the vertical component of the effective mean Lorentz force; see the second term on the right-hand side of equation (10). Our DNS shows that the dimensionless quantity $q_{\rm g}$ is mostly positive (see Figs 4 and 5), which implies that this effect increases the negative contribution of anisotropic turbulent convection to the effective mean magnetic pressure. Note that the DNS in stratified forced turbulence of BKKR has not found strong anisotropic contributions as characterized by the term $q_{\rm g}$. On the other hand, the negative contribution of anisotropic turbulent convection to the effective mean magnetic tension, as characterized by positive values of $q_{\rm s}$, has neither been found in our DNS (see Figs 6 and 7) nor in those of BKKR.

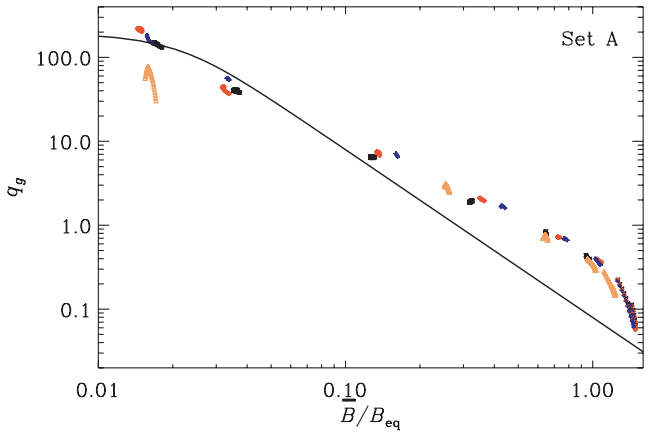

Figure 4. $q_{\rm g}$ as a function of the mean magnetic field from runs A1–A29. The symbols and colours are the same as in Fig. 2. The solid line applies to the fit parameters $q_{\rm g0} = 200$ and $B_{\rm g} = 0.025B_{\rm eq}$.

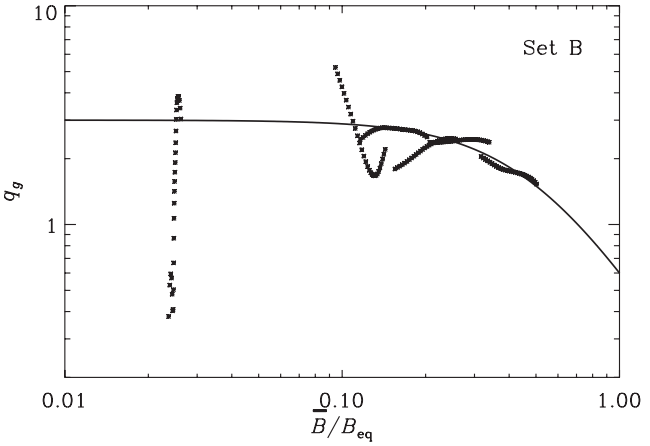

Figure 5. Same as Fig. 4 but for runs B1–B8. The fit parameters are $q_{\rm g0} = 3$ and $B_{\rm g} = 0.5B_{\rm eq}$.

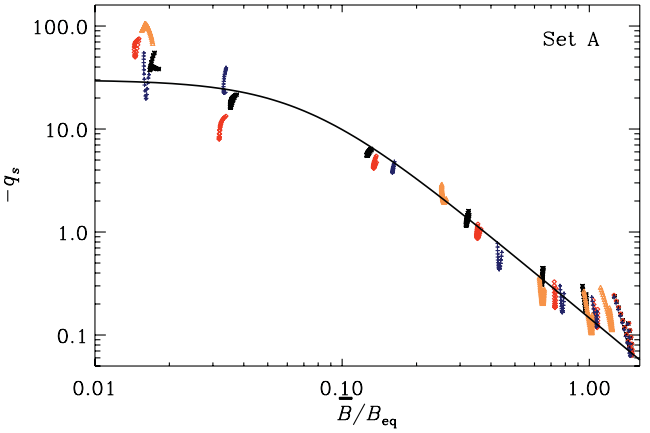

Figure 6. Effective magnetic tension parameter as a function of the mean magnetic field from runs A1–A29. The symbols and colours are the same as in Fig. 2. The solid line applies to the fit parameters $q_{\rm s0} = -30$ and $B_{\rm s} = 0.07B_{\rm eq}$.

In Fig. 8 we show the magnetic field component B_x from run B3 with an imposed horizontal magnetic field $\overline{\boldsymbol{B}} \approx 0.23B_{\rm eq}\hat{\boldsymbol{x}}$. The structure of the magnetic field, however, does not show clear signs of magnetic flux concentrations in the DNS. Even after additional averaging over time and along the x-direction no spatial modulation of the magnetic field is seen. The simulations of Brandenburg et al. (2011) strongly suggest that the reason for this is related to lack of scale separation. As demonstrated in fig. 17 of BKKR, at larger scale separation the turbulent diffusivity on the scale of the domain becomes weak enough to allow for the development of large-scale magnetic structures.

4 ENTROPY EVOLUTION IN MEAN-FIELD MODELS

4.1 Mean-field equations

We now apply a mean-field model similar to that of BKR for adiabatic stratification and those of BKKR and Kemel et al. (2012b)

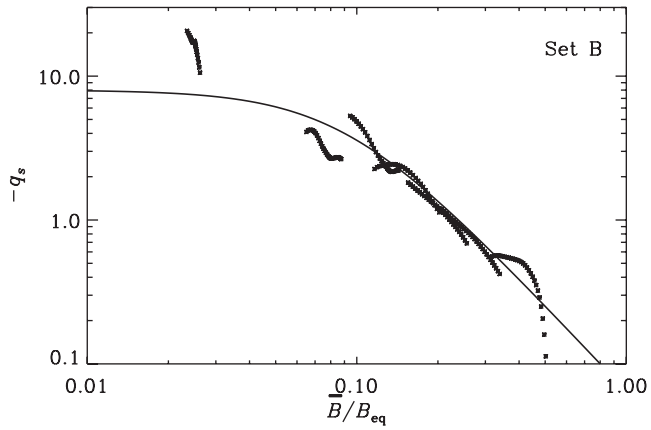

Figure 7. Same as Fig. 6 but for runs B1–B8. The solid line applies to the fit parameters $q_{s0} = -8$ and $B_s = 0.09B_{eq}$.

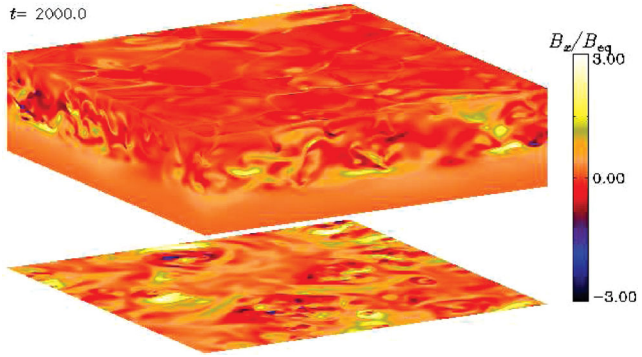

Figure 8. Magnetic field component B_x from run B3 with an imposed horizontal field $B_0\hat{\boldsymbol{x}}$ at Rm = 45, Pm = 1, a density contrast of 320, and $B_0/B_{eq} = 0.23$.

for isothermal stratification. Both types of models are in principle able to display a large-scale instability provided the domain is big compared with the typical size of turbulent eddies, i.e. the scale separation ratio is large. In the mean-field calculations of BKKR it was shown that in models with too low scale separation ratio the turbulent magnetic diffusivity and turbulent viscosity (which are proportional to the scale of the energy-carrying turbulent eddies) was too large, so the instability is too weak or not excited. Even if the scale separation ratio is big enough, the instability can only develop if $\mathrm{d}\mathcal{P}_{\rm eff}/\mathrm{d}\beta^2$, taken at the value of the imposed field, is negative inside the domain (BKKR; Kemel et al. 2012b). If these conditions are satisfied, the maximum growth rate of the instability was shown to be independent of the strength of the imposed field for models with isothermal background stratification.

Whenever the instability is possible, its non-linear development appears to be rather similar for isothermal and adiabatic background stratification. In particular, Kemel et al. (2012b) found that for $q_s = 0$, the eigenmode shows no variation along the direction of the applied magnetic field. Conversely, if the model is two-dimensional with no extent in the y-direction, which will be assumed here, the results are independent of the value of q_{s0}, so we take in the following $q_{s0} = 0$. Furthermore, for large magnetic Reynolds number, simulations at different scale separation ratios (Kemel et al. 2012a) suggest $q_{p0} = 40$ and $\beta_p = 0.05$, which were therefore also the fiducial parameters used in the study of Kemel et al. (2012b) and will therefore also be used here. The results of the DNS presented here suggest somewhat larger values of q_{p0} of 130 for set A and 95 for set B, but this could be a consequence of intermediate magnetic Reynolds numbers for which q_{g0} is known to reach a peak (see fig. 10 of Kemel et al. 2012a). The dependence on the parameter q_{g0} has not yet previously been determined, so this will be done at the end of Section 4.3. In all other cases, we keep $q_{g0} = 0$. The imposed field strength B_0 is chosen such that the minimum of $\mathcal{P}_{\rm eff}$ occurs near the top boundary and thus $\mathrm{d}\mathcal{P}_{\rm eff}/\mathrm{d}\beta^2 < 0$ in the domain. We express B_0 in units of $B_{eq0} = B_{eq}(0)$, which is the equipartition field strength at $z = 0$.

The novel aspect of the present work is that an evolution equation for the mean specific entropy is included. Thus, we solve the following system of equations for the mean vector potential $\overline{\boldsymbol{A}}$, the mean velocity $\overline{\boldsymbol{U}}$, the mean density $\overline{\rho}$ and the mean specific entropy $\overline{s}$, in the form

$$\frac{\partial \overline{\boldsymbol{A}}}{\partial t} = \overline{\boldsymbol{U}} \times \overline{\boldsymbol{B}} - \eta_{\rm T}\mu_0 \overline{\boldsymbol{J}}, \tag{32}$$

$$\frac{\partial \overline{\boldsymbol{U}}}{\partial t} = -\overline{\boldsymbol{U}} \cdot \nabla \overline{\boldsymbol{U}} - \frac{1}{\overline{\rho}}\nabla \overline{p} + \boldsymbol{g} + \overline{\boldsymbol{\mathcal{F}}}^{\rm M} + \overline{\boldsymbol{\mathcal{F}}}^{\rm K}_{\rm tot}, \tag{33}$$

$$\frac{\partial \overline{\rho}}{\partial t} = -\overline{\boldsymbol{U}} \cdot \nabla \overline{\rho} - \overline{\rho}\nabla \cdot \overline{\boldsymbol{U}}, \tag{34}$$

$$\frac{\partial \overline{s}}{\partial t} = -\overline{\boldsymbol{U}} \cdot \nabla \overline{s} - \frac{1}{\overline{\rho}\,\overline{T}}\nabla \cdot \boldsymbol{F} + 2\nu_{\rm T}\overline{\boldsymbol{S}}^2 + \frac{\eta_{\rm t}\mu_0}{\overline{\rho}}\overline{\boldsymbol{J}}^2 - \frac{1}{\overline{T}}\Gamma_{\rm cool}, \tag{35}$$

where $\overline{\boldsymbol{B}} = \boldsymbol{B}_0 + \nabla \times \overline{\boldsymbol{A}}$ is the mean magnetic field including the imposed field, $\eta_{\rm T} = \eta_{\rm t} + \eta$ and $\nu_{\rm T} = \nu_{\rm t} + \nu$ are total (turbulent and microphysical) magnetic diffusivity and viscosity, respectively, the effective mean Lorentz force is given by equation (10), and the total viscous force, $\overline{\boldsymbol{\mathcal{F}}}^{\rm K}_{\rm tot} = (2/\overline{\rho})\nabla \cdot (\overline{\rho}\nu_{\rm T}\overline{\boldsymbol{S}})$. We assume $\nu_{\rm t}/\eta_{\rm t} = 1$ for the *turbulent* magnetic Prandtl number. The mean temperature obeys $(\gamma - 1)c_{\rm p}\overline{T} = \gamma\overline{p}/\overline{\rho} = c_{\rm s}^2$. The boundary conditions are stress-free for the velocities, and perfect conductor boundary conditions for the magnetic field as in previous mean field models. In the following, we consider two types of background stratification: isothermal and adiabatic.

4.2 Isothermal background stratification

We begin by assessing the effects of entropy evolution in the isothermal models studied by BKKR and Kemel et al. (2012b). In general, the gas will not stay isothermal, because the temperature changes due to adiabatic expansion and compression. Indeed, in an isothermally stratified layer a rising blob cools adiabatically, becomes denser or heavier, and thus experiences a restoring force with the Brunt–Väisälä frequency N, where $N^2 = -\boldsymbol{g} \cdot \nabla \overline{s}/c_{\rm p} = (\gamma - 1)g/\gamma H_\rho$, with H_ρ being the density scale height. It turns out that in such a case the negative effective magnetic pressure instability can be stabilized. To study this in more detail, we allow for cooling term of the form $\Gamma_{\rm cool} = (\overline{T} - T_0)/c_{\rm p}\overline{T}\tau$, where $\overline{T}$ is the mean temperature, T_0 is the reference temperature of the layer and τ is a cooling time. For the energy flux $\boldsymbol{F}$, we assume $\boldsymbol{F} = -K\nabla\overline{T}$.

In Fig. 9 we show the evolution of the normalized rms value of the mean flow, $\overline{U}_{\rm rms}/u_{\rm rms}$, for different cooling times τ and $B_0 = 0.1B_{eq0}$. The instability is found to operate only when τN is less than a critical value of the order of unity. The largest growth rate seen in Fig. 9 is $\approx 60\eta_{\rm t}k_1^2$. The earlier results with an isothermal equation of state are recovered in the limit $\tau N \to 0$, in which case a growth rate of $\approx 110\eta_{\rm t}k_1^2$ is found; see fig. 4 of Kemel et al. (2012b), where the growth rate is normalized by $(\nu_{\rm t} + \eta_{\rm t})k_1^2$.

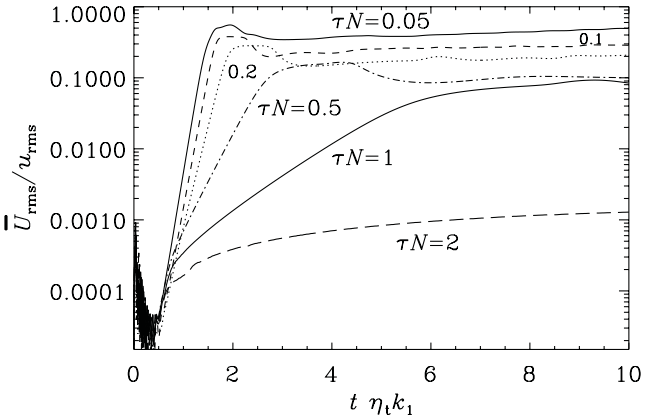

Figure 9. Evolution of $\overline{U}_{\rm rms}/u_{\rm rms}$ for different cooling times τ normalized by the Brunt–Väisälä frequency N.

4.3 Adiabatic background stratification

Owing to the stabilizing properties of stable stratification, we now study the evolution of the instability in an adiabatically stratified layer, where this stabilizing effect is absent and the squared sound speed is given by $c_{\rm s}^2 = g(z - z_\infty)$. Our set-up is similar to that of BKR, who considered a reference height $z = 0$, at which initially $c_{\rm s} = c_{\rm s0}$ and $\rho = \rho_0$, where $c_{\rm s0}$ and ρ_0 are normalization constants. Length is normalized with respect to the density scale height $H_{\rho 0} = c_{\rm s}^2/g$ at $z = 0$. This implies that $z_\infty = (3/2)H_{\rho 0}$. In BKR, the domain extended in the x-direction from $-5H_{\rho 0}$ to $+5H_{\rho 0}$, but the resulting horizontal wavelength of the fastest growing eigenfunction was then about half the x extent. Therefore, we consider here a smaller domain, with $-3H_{\rho 0} < x < 3H_{\rho 0}$ and $-5H_{\rho 0} < z < H_{\rho 0}$. As in BKR, we choose $B_0/B_{\rm eq0} = 0.01$. Here we use $\boldsymbol{F} = -\chi_{\rm t}\overline{\rho}\,\overline{T}\nabla\overline{s}$ for the energy flux which is appropriate for a turbulent layer, and $\nu_{\rm t}/\chi_{\rm t} = 1$ is the turbulent Prandtl number, where $\chi_{\rm t}$ is the turbulent heat conductivity.

It turns out that heating is weak, so we ignore the cooling term, i.e. $\tau \to \infty$. In Fig. 10 we show velocity vectors together with $\overline{B}_y$ as well as $\overline{s}$ for three different times close to saturation. Note that there is a weak enhancement of $\overline{s}$ at the location where the instability develops a positive maximum. This mean entropy enhancement is associated with turbulent viscous heating, in particular the contribution $\sim \nu_{\rm T}(\nabla \cdot \overline{\boldsymbol{U}})$, which is important near the surface, even though the magnetic flux concentration later descends to greater depths.

Finally, we use this model to assess the dependence on the parameter $q_{\rm g0}$, which can directly contribute to the negative effective magnetic pressure instability. According to the DNS, we have $q_{\rm g0} \approx 200$ with $\beta_{\rm g} \equiv B_{\rm g}/B_{\rm eq} = 0.025$ for set A (Fig. 4) and $q_{\rm g0} \approx 3$ with $\beta_{\rm g} = 0.5$ for set B (Fig. 5). Fig. 11 indicates that the $q_{\rm g}$ effect would be detrimental to the instability for set A, and negligible for set B. Furthermore, near $q_{\rm g0} = 0$ the dependence of the growth rate on $q_{\rm g0}$ is not monotonous: for $q_{\rm g0} = 3$ the growth rate is slightly enhanced and for $q_{\rm g0} = 10$ it is decreased, but enhanced for $q_{\rm g0} = -10$ by a similar amount. The saturation level is only weakly affected by the value of $q_{\rm g0}$. We also checked that, as expected from earlier work (Kemel et al. 2012b), the value of $q_{\rm s0}$ affects neither the growth rate nor the saturation value of $\overline{U}_{\rm rms}$.

5 CONCLUSIONS

The present simulations have demonstrated that for weak stratification, and magnetic fields less than the equipartition value, a destabilising contribution to the mean Lorentz force is obtained in the presence of turbulent convection. A similar effect is found for strong density stratification, although the effect is weaker and limited to a narrower range in magnetic fields. Our DNS results agree at least qualitatively with those from non-stratified (BKR) and stratified (BKKR) forced turbulence and with theoretical predictions (Rogachevskii & Kleeorin 2007), although the minimum effective magnetic pressure can now be even more negative and the range where it is negative extends now to nearly $0.5B_{\rm eq}$.

Such negative contributions to the effective magnetic pressure facilitate an instability that can lead to the generation of flux concentrations from an initially uniform magnetic field. This could explain the origin of active regions and sunspots. However, no clear signs of instability are found from DNS in turbulent convection.

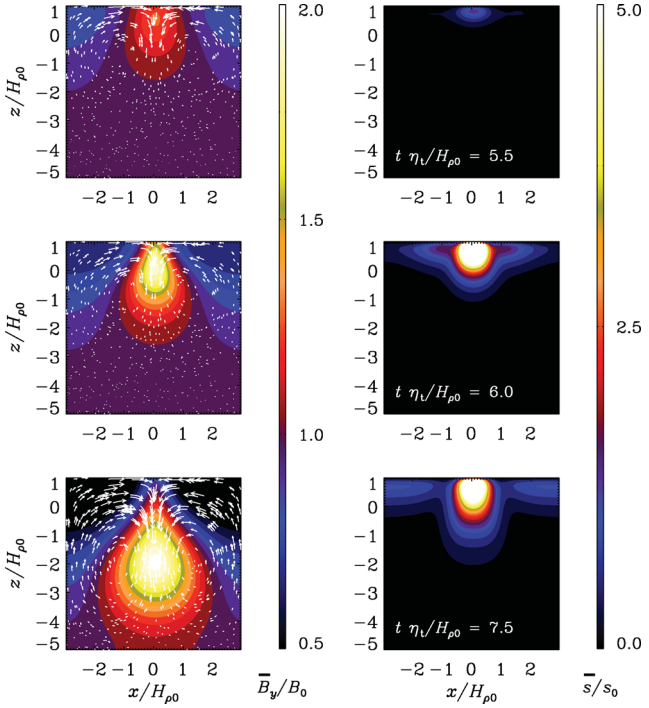

Figure 10. Velocity vectors superimposed on colour scale representations of $\overline{B}_y$ (left) as well as colour scale representations of $\overline{s}$ (right) for three different times close to saturation. Specific entropy is shown in units of $s_0 = 10^{-4}c_{\rm p}$.

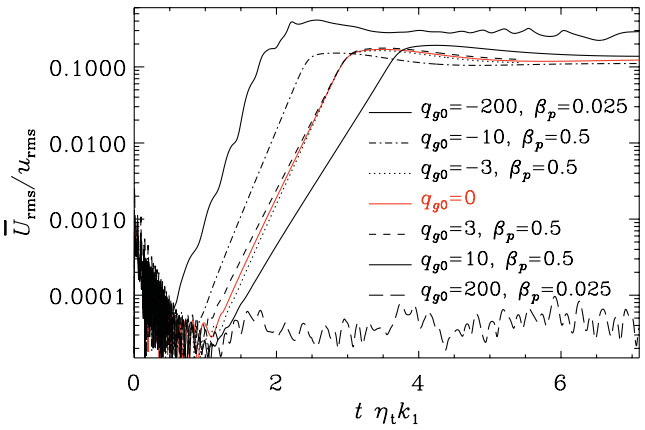

Figure 11. Evolution of $\overline{U}_{\rm rms}/u_{\rm rms}$ for adiabatic stratification using different combinations of $q_{\rm g0}$ and $\beta_{\rm g} = B_{\rm g}/B_{\rm eq}$.

A possible reason is that the scale separation in the DNS is insufficient, as has been demonstrated by Brandenburg et al. (2011), who found conclusive evidence of the operation of the negative effective magnetic pressure instability in DNS in forced turbulence with a scale separation ratio of 15, using also spatial–temporal averaging. For a scale separation ratio of 30, the effect is stronger and flux concentrations can already be seen without averaging (Kemel et al. 2012a). On the other hand, if the scale separation ratio is as low as 5, no flux concentrations have been found (BKKR).

So far, all studies of the negative effective magnetic pressure effect have only considered the case of a horizontal mean field. While this is the most relevant case in view of applications to stars with differential rotation, the case of a vertical field is also of interest and might lead to additional effects. Another important extension of our work is to the case where small-scale dynamo action becomes important. This effect is expected to lower the relative importance of the negative effective magnetic pressure effect, although this will depend on the value of the magnetic Prandtl number, which is yet another important parameter whose effect on the instability is not yet sufficiently well understood. Finally, we have mentioned the possibility of finite scale separation effects, which would mean that the scale of the magnetic structure will be important in determining the efficiency of the negative effective magnetic pressure effect. The hope is that such considerations will provide some insight as to why we have not yet seen clear evidence for the negative effective magnetic pressure instability in the present DNS. Once these various issues are better understood, it becomes timely to improve mean-field modelling. Obviously, all the mean-field models of the negative effective magnetic pressure instability have ignored realistic profiles of density and turbulent intensity. Also, the mean-field models should really be three-dimensional to include the possibility that magnetic structures break up along the direction of the mean field and form bipolar regions, as was seen in models of BKR.

ACKNOWLEDGMENTS

We acknowledge the NORDITA dynamo programmes of 2009 and 2011 for providing a stimulating scientific atmosphere. The numerical simulations were performed with the supercomputers hosted by CSC – IT Center for Science in Espoo, Finland, who are administered by the Finnish Ministry of Education. Financial support from the Academy of Finland grant Nos. 121431, 136189 (PJK) and 112020 (MJM), the Swedish Research Council grant 621-2007-4064, and the European Research Council under the AstroDyn Research Project 227952 is acknowledged.

REFERENCES

Arlt R., Sule A., Rüdiger G., 2005, A&A, 441, 1171
Benevolenskaya E. E., Hoeksema J. T., Kosovichev A. G., Scherrer P. H., 1999, ApJ, 517, L163
Brandenburg A., 2005, ApJ, 625, 539
Brandenburg A., Subramanian K., 2005, Phys. Rep., 417, 1
Brandenburg A., Kleeorin N., Rogachevskii I., 2010, Astron. Nachr., 331, 5 (BKR)
Brandenburg A., Kemel K., Kleeorin N., Mitra D., Rogachevskii I., 2011, ApJ, 740, L50
Brandenburg A., Kemel K., Kleeorin N., Rogachevskii I., 2012, ApJ, preprint (arXiv:1005.5700) (BKKR)
D'Silva S., Choudhuri A. R., 1993, A&A, 272, 621
Dikpati M., Charbonneau P., 1999, ApJ, 518, 508
Guerrero G., Käpylä P. J., 2011, A&A, 533, A40
Hughes D. W., 2007, in Hughes D. W., Rosner R., Weiss N. O., eds, The Solar Tachocline. Cambridge Univ. Press, Cambridge, p. 275
Käpylä P. J., Korpi M. J., Tuominen I., 2006, Astron. Nachr., 327, 884
Käpylä P. J., Korpi M. J., Brandenburg A., 2008, A&A, 491, 353
Käpylä P. J., Korpi M. J., Brandenburg A., 2009, ApJ, 697, 1153
Käpylä P. J., Korpi M. J., Brandenburg A., 2010, MNRAS, 402, 1458
Kemel K., Brandenburg A., Kleeorin N., Mitra D., Rogachevskii I., 2012a, Solar Phys., preprint (arXiv:1112.0279)
Kemel K., Brandenburg A., Kleeorin N., Rogachevskii I., 2012b, Astron. Nachr., 333, 95
Kitiashvili I. N., Kosovichev A. G., Wray A. A., Mansour N. N., 2010, ApJ, 719, 307
Kleeorin N., Rogachevskii I., 1994, Phys. Rev. E, 50, 2716
Kleeorin N. I., Rogachevskii I. V., Ruzmaikin A. A., 1989, Sov. Astron. Lett., 15, 274
Kleeorin N. I., Rogachevskii I. V., Ruzmaikin A. A., 1990, Sov. Phys. JETP, 70, 878
Kleeorin N., Mond M., Rogachevskii I., 1996, A&A, 307, 23
Krause F., Rädler K.-H., 1980, Mean-field Magnetohydrodynamics and Dynamo Theory. Pergamon Press, Oxford
Martínez J., Hansteen V., Carlson M., 2008, ApJ, 679, 871
Moffatt H. K., 1978, Magnetic Field Generation in Electrically Conducting Fluids. Cambridge Univ. Press, Cambridge
Parker E. N., 1955, ApJ, 121, 491
Parker E. N., 1979, Cosmical Magnetic Fields. Oxford Univ. Press, New York
Parker E. N., 1982, ApJ, 256, 302
Parker E. N., 1984, ApJ, 283, 343
Pulkkinen P., Tuominen I., 1998, A&A, 332, 748
Rempel M., Schüssler M., Knölker M., 2009, ApJ, 691, 640
Rogachevskii I., Kleeorin N., 2007, Phys. Rev. E, 76, 056307
Rüdiger G., Hollerbach R., 2004, The Magnetic Universe. Wiley-VCH, Weinheim
Schüssler M., Vögler A., 2006, ApJ, 641, L73
Schüssler M., Caligari P., Ferriz-Mas A., Moreno Insertis F., 1994, A&A, 281, L69
Spiegel E. A., Weiss N. O., 1980, Nat, 287, 616
Spruit H. C., 1981, A&A, 98, 155
Stein R. F., Lagerfjärd A., Nordlund Å., Georgobiani D., 2011, Solar Phys., 268, 271
Stix M., 1976, A&A, 47, 243
Tao L., Weiss N. O., Brownjohn D. P., Proctor M. R. E., 1998, ApJ, 496, L39
Tian C., Petrovay K., 2012, A&A, submitted (arXiv:1105.5590)
Tobias S. M., Weiss N. O., 2007, in Hughes D. W., Rosner R., Weiss N. O., eds, The Solar Tachocline. Cambridge Univ. Press, Cambridge, p. 319
Ustyugov S. D., 2009, in Dikpati M., Arentoft T., González Hernández I., Lindsey C., Hill F., eds, ASP Conf. Ser. Vol. 416, Solar-Stellar Dynamos as Revealed by Helio- and Asteroseismology: GONG 2008/SOHO 21. Astron. Soc. Pac., San Francisco, p. 427

This paper has been typeset from a TEX/LATEX file prepared by the author.